Eur. Phys. J. C (2010) 68: 183–195
DOI 10.1140/epjc/s10052-010-1306-6

THE EUROPEAN PHYSICAL JOURNAL C

Regular Article - Theoretical Physics

Strong-coupling study of the Gribov ambiguity in lattice Landau gauge

Axel Maas[1], **Jan M. Pawlowski**[2,3], **Daniel Spielmann**[2,3,a], **André Sternbeck**[4,5], **Lorenz von Smekal**[6]

[1]Institut für Physik, Karl-Franzens Universität Graz, Universitätsplatz 5, 8010 Graz, Austria
[2]Institut für Theoretische Physik, Universität Heidelberg, Philosophenweg 16, 69120 Heidelberg, Germany
[3]ExtreMe Matter Institute EMMI, GSI Helmholtzzentrum für Schwerionenforschung, Planckstr. 1, 64291 Darmstadt, Germany
[4]Centre for the Subatomic Structure of Matter, University of Adelaide, SA 5005, Adelaide, Australia
[5]Institut für Theoretische Physik, Universität Regensburg, 93040 Regensburg, Germany
[6]Institut für Kernphysik, Technische Universität Darmstadt, Schlossgartenstr. 9, 64289 Darmstadt, Germany

Received: 13 January 2010 / Published online: 13 April 2010

Abstract We study the strong-coupling limit $\beta = 0$ of lattice SU(2) Landau gauge Yang–Mills theory. In this limit the lattice spacing is infinite, and thus all momenta in physical units are infinitesimally small. Hence, the infrared behavior can be assessed at sufficiently large lattice momenta. Our results show that at the lattice volumes used here, the Gribov ambiguity has an enormous effect on the ghost propagator in all dimensions. This underlines the severity of the Gribov problem and calls for refined studies also at finite β. In turn, the gluon propagator only mildly depends on the Gribov ambiguity.

1 Introduction

The study of the long-range behavior of QCD Green's functions is one path towards the understanding of confinement [1, 2]. In particular, the confining properties of QCD are directly reflected in the behavior of the Landau gauge gluon and ghost propagators at asymptotically low momenta [3]. Furthermore, confinement, as signaled by an unbroken center symmetry, can also be shown to be a direct consequence of these properties [4].

However, implementing Landau gauge as in the perturbative regime is not sufficient to uniquely fix the infrared behavior of Green's functions because of the Gribov–Singer ambiguity [5, 6]. Using functional methods, one finds a one-parameter family of solutions which can be classified by the zero momentum value of the ghost propagator [7, 8]. These can be obtained by specifying a non-perturbative renormalization condition [7].

The one-parameter family of solutions contains the *scaling solution* as a limiting special case [7], which is characterized by an infrared divergent ghost dressing function, and an infrared suppressed and likely vanishing gluon propagator, see e.g. [1, 9–17]. In contrast, the other members of the family with an infrared finite ghost dressing function necessarily come along with an infrared finite gluon propagator, see e.g. [7, 8, 18–26]. These are called the *decoupling solutions* [7]. Both terms are more precisely defined in Sect. 2.

These Green's functions have also been determined on the lattice. By now it is well established that standard lattice gauge fixings lead to a decoupling-type behavior, see e.g. [27–37], though not unanimously [38, 39]. Moreover, investigations of the Gribov–Singer ambiguity in this setting, [27–31, 35–37, 40–45], so far only led to relatively small, quantitative effects.

However, recently alternative gauge fixing procedures have been devised that directly make use of the Gribov–Singer ambiguity [46]. Here, one selects different non-perturbative completions of the Landau gauge by constricting the ghost propagator in the zero momentum limit to be as close as possible to a fixed value. Such a procedure samples Gribov copies differently than a standard gauge fixing. It introduces an additional parameter which plays a role analogous to the non-perturbative renormalization condition of the continuum studies. The interpretation here is that this free parameter is therefore linked to the residual gauge freedom of the Landau gauge.

Note that the qualitatively different infrared solutions, decoupling and scaling, signal different realizations of the global part of the gauge fixing. At the level of gauge-invariant observables they have to be equivalent. One particular difference is the structure of the Becchi–Rouet–Stora–Tyutin (BRST) symmetry. If a given non-perturbative com-

[a] e-mail: d.spielmann@thphys.uni-heidelberg.de

pletion of the Landau gauge is to have a global BRST symmetry then the Kugo–Ojima confinement criterion requires that the corresponding Landau gauge ghost propagator is infrared enhanced, corresponding to the scaling solution [7, 47]. On the other hand, in the decoupling case, the infrared ghost propagator is essentially massless. In standard Faddeev–Popov theory, the corresponding massless asymptotic ghost states, albeit being unphysical, would then contribute to the global gauge charges and lead to a spontaneous breaking of the global gauge symmetry much like what one expects for theories with a Higgs mechanism. When there is no Higgs mechanism, and thus no physical vector field in the gauge boson sector, this breaking is most likely artificial and due to a non-perturbative breakdown of BRST symmetry itself [23, 24, 48–55]. At present, the only solution which is consistent with an unbroken BRST symmetry is thus the scaling solution. Note that other BRST formulations might exist, in which the massless ghosts of the decoupling solutions would not automatically lead to BRST breaking. However, such a formulation is still lacking, but investigations along the lines of [51] appear promising.

On the lattice, the only way that is currently known to define BRST symmetry in presence of Gribov copies and thus fully non-perturbatively is based on defining gauge fields by stereographic projection. This avoids the perfect cancelation of Gribov copies and the Neuberger $0/0$ problem of lattice BRST, while it nevertheless reduces to the standard BRST symmetry in the continuum limit, [56–60].

As noted above, for studying the long-range behavior of the Landau gauge gluon and ghost propagators on the lattice, it is useful to employ the strong-coupling limit [42–44, 61, 62]. In our present work we use the strong-coupling limit $\beta \to 0$ for pure SU(2) lattice gauge theory in $d = 2$ and 3 dimensions. This limit can be interpreted as the limit of infinite lattice spacing, $a \to \infty$, at a fixed physical scale as set, e.g., by the string tension. Alternatively, when considering all momenta in lattice units, $q \sim 1/a$, the same limit can also be interpreted as the hypothetical limit in which the physical scale is sent to infinity, i.e., formally as $\Lambda_{\mathrm{QCD}} \to \infty$. Both interpretations are equivalent. They are based on taking the limit of the function $a(\beta)$ for $\beta \to 0$. Other ways to assign a scale to the theory at $\beta = 0$ are possible [61, 63], but they require different prescriptions. For the limit $\beta \to 0$ adopted here, all momenta and masses in lattice units $1/a$ are infinitely small relative to the physical scale of the theory which is precisely what we need for an analysis of the asymptotic infrared behavior of its correlation functions. It is therefore best suited to isolate this behavior from finite-volume effects.

In recent studies [42–44, 61] the $\beta \to 0$ limit was first investigated only in four dimensions [42–44] and then to some extent also in lower dimensions [61]. The results of both studies were compatible with a scaling behavior for the gluon propagator for intermediate to large momenta and a decoupling behavior at small momenta, where 'large' and 'small' in the strong-coupling limit always refers to lattice units. It has moreover been shown in [42–44] that the mass parameter related to the low-momentum decoupling tail can be changed by choosing different definitions of the gluon field, which should be equivalent in the continuum limit. For non-vanishing lattice spacing a, however, these correspond to different lattice implementations of the Landau gauge [58]. If some of these differences remain in the continuum limit that would strengthen the hypothesis [7, 45, 46] of a residual gauge freedom related to the one-parameter family of solutions observed in the continuum. In any case, the lattice discretization dependence adds to the puzzle of the global properties of Landau gauge Yang–Mills theory.

The interpretation of the data for the ghost propagator has always been even less conclusive, and did not allow a direct determination of local scaling coefficients. This led to a more indirect interpretation of the data. In [42–44] it was concluded that the ghost data at larger lattice momenta could be consistent with the scaling behavior observed in the gluon propagator. However, it was not possible to extract a firm value for the scaling exponent from the ghost data for any reasonably wide range of lattice momenta. In turn, the authors of [61] assessed the evidence of a logarithmic momentum dependence and argued in favor of decoupling at all lattice momenta for Landau gauge Yang–Mills theory in three and four dimensions in the strong-coupling limit. It was also frequently claimed that the scaling solution is realized in two dimensions in agreement with the arguments in [64] and the lattice data of [32, 37, 65].

In this paper we present results with much improved statistical accuracy in two and three dimensions. We also provide a more detailed study of the systematic uncertainties, see Appendices A and B, and of the relevance of the Gribov ambiguity, see Sect. 3 and parts of Sect. 4.

Our results are presented in Sect. 4. For the gluon propagator we confirm the scaling results of [42–44, 61] at intermediate lattice momenta. In particular, we obtain fairly stable scaling exponents also with the local analysis of [61]. The values for the exponents tend to decrease somewhat at large lattice momenta, and as in the previous studies we observe decoupling at small momenta, at least in three dimensions.

A qualitatively new and perhaps surprising behavior is seen in the ghost propagator which shows a very strong sensitivity to Gribov copies at low momenta. This entails that we still have to work on a better understanding of the global properties of Landau gauge QCD. In particular our analysis shows that a proper treatment of Gribov copies in the thermodynamical limit of Landau gauge lattice Yang–Mills theory has not been achieved yet. Subject to the sampling of Gribov copies the ghost propagator can be tuned

to also show a scaling behavior for intermediate momenta. The general trend is that even a drastic over-scaling is obtained if enough gauge copies are taken into account in the search for the maximally achievable infrared enhancement. In fact, the possibility of such an over-scaling has also been observed in continuum Landau gauge Yang–Mills theory on the torus [66]. Here, we moreover demonstrate that this peculiar behavior arises already in two dimensions where infrared scaling was supposed to be quite well established. We find that the two-dimensional ghost propagator shows the same apparently unconstrained infrared behavior as that in higher dimensions, and that there is thus no qualitative difference between two and higher dimensions as long as sufficiently many Gribov copies are present, as has been suspected [45, 46].

In the summary in Sect. 5 we are led to conclude that our analysis clearly shows the direct relation between the ambiguities in the ghost propagator at low and intermediate momenta and the Gribov ambiguity. In our opinion this ambiguity is much more than an artificial problem of this unphysical limit. In fact, Gribov copies at finite lattice coupling β will remain to affect the infrared behavior of Green's functions as long as they are present in the strong-coupling limit. To resolve it there will certainly be more cost-efficient than to try to reach the continuum limit in a sufficiently large physical volume by brute force, though this is attempted as well [67].

2 Infrared scaling and decoupling

The Landau gauge gluon propagator, in (Euclidean) momentum space, is parameterized by a single dressing function Z,

$$D^{ab}_{\mu\nu}(p) = \delta^{ab}\left(\delta_{\mu\nu} - \frac{p_\mu p_\nu}{p^2}\right)\frac{Z(p^2)}{p^2}, \tag{1}$$

and the ghost propagator by a corresponding dressing function G,

$$D^{ab}_{G}(p) = -\delta^{ab}\frac{G(p^2)}{p^2}. \tag{2}$$

For their infrared behavior, i.e., that of $Z(p^2)$ and $G(p^2)$ for $p^2 \to 0$, we consider the two possibilities of scaling and decoupling. Occasionally, we also use $D_{gl} = Z(p^2)/p^2$ and $D_{gh} = G(p)^2/p^2$.

2.1 Scaling

The prediction of [9–13, 68] amounts to infrared asymptotic forms

$$Z\big(p^2\big) \sim \big(p^2/\Lambda^2_{\mathrm{QCD}}\big)^{2\kappa_Z+\frac{4-d}{2}}, \tag{3a}$$

$$G\big(p^2\big) \sim \big(p^2/\Lambda^2_{\mathrm{QCD}}\big)^{-\kappa}, \tag{3b}$$

for $p^2 \to 0$, which are both determined by an unique critical infrared exponent

$$\kappa_Z = \kappa, \tag{4}$$

with $(d-2)/4 \le \kappa < d/4$. Furthermore it has been proven in [4] that the scaling solution is confining for

$$\kappa > \frac{d-3}{4}. \tag{5}$$

Under a mild regularity assumption on the ghost–gluon vertex [12], the value of this exponent is furthermore obtained in four dimensions as [11, 12]

$$\kappa = (93 - \sqrt{1201})/98 \approx 0.595, \tag{6}$$

which is confinement according to (5). The corresponding values in lower dimensions are $\kappa = 1/5$ $(d = 2)$ and $\kappa \approx 0.3976$ $(d = 3)$ which also satisfy (5). The conformal nature of this infrared behavior in the pure Yang–Mills sector of Landau gauge QCD is evident in the generalization to arbitrary gluonic correlations [14]: an uniform infrared limit of one-particle irreducible vertex functions $\Gamma^{m,n}$ with m external gluon legs and n pairs of ghost/anti-ghost legs, in four dimensions of the form

$$\Gamma^{m,n} \sim \big(p^2/\Lambda^2_{\mathrm{QCD}}\big)^{(n-m)\kappa}, \tag{7}$$

when all $p_i^2 \propto p^2 \to 0$, $i = 1, \ldots, 2n+m$. In particular, the ghost–gluon vertex is then infrared finite (with $n = m = 1$), in agreement with its STI [69], and the non-perturbative running coupling introduced in [9, 10] via the definition

$$\alpha_s\big(p^2\big) = \frac{g^2}{4\pi}Z\big(p^2\big)G^2\big(p^2\big) \tag{8}$$

approaches an infrared fixed point, $\alpha_s \to \alpha_c$ for $p^2 \to 0$ in $d = 4$. For arbitrary dimensions, trivial kinematic factors lead to an infrared fixed point for the effective coupling

$$\alpha_e\big(p^2\big) = p^{d-4}\alpha_s\big(p^2\big), \tag{9}$$

with $\alpha_e(0) = \alpha_c$. If the ghost–gluon vertex is regular at $p^2 = 0$, its value is in four dimensions [12]

$$\alpha_c = \frac{8\pi}{N_c}\frac{\Gamma^2(\kappa-1)\Gamma(4-2\kappa)}{\Gamma^2(-\kappa)\Gamma(2\kappa-1)} \approx \frac{9}{N_c} \times 0.99. \tag{10}$$

Comparing the infrared scaling behavior of Dyson–Schwinger equation (DSE) and functional renormalization group equation (FRGE) for solutions of the form of (3), it has been shown that in presence of a single scale, the QCD scale Λ_{QCD}, the solution with the infrared behavior (4) and (7), with positive κ, is unique [15, 16, 70, 71]. It is nowadays being called the *scaling solution*.

2.2 Decoupling

This uniqueness proof does not rule out, however, the possibility of a solution with an infrared finite gluon propagator, as arising from a transverse gluon mass M, which then leads to an essentially free ghost propagator, with the free massless-particle singularity at $p^2 = 0$, i.e.,

$$Z(p^2) \sim p^2/M^2, \quad \text{and} \quad G(p^2) \sim \text{const.} \tag{11}$$

for $p^2 \to 0$ [7, 8, 18–26]. The constant contribution to the zero-momentum gluon propagator, $D(0) = 1/M^2$, thereby necessarily leads to an infrared constant ghost renormalization function G. This solution corresponds to $\kappa_Z = 1/2$ and $\kappa = 0$, and it has been proven in [4] that it is confining. It does not satisfy the scaling relations (4) or (7). This is since the transverse gluons decouple for momenta $p^2 \ll M^2$, below the independent second scale given by their mass M. It is thus not within the class of scaling solutions considered above, and it is termed the *decoupling solution* in contradistinction. The renormalization group invariant (8) shows this decoupling as it tends to zero in the infrared. Alternatively, we can define a running coupling analogously to that in massive theories. By fixing one overall free parameter this definition leads to a coupling which even quantitatively resembles the fixed-point coupling in the scaling case. This definition has been given explicitly in [7] and similarly been used since then [25, 26].

3 Gauge fixing and the ghost propagator

The functional equations of continuum quantum field theory, such as DSEs and FRGEs, admit a one-parameter family of solutions [7]. The free parameter can be chosen as the value of the ghost dressing function at vanishing momentum. It fixes an ambiguity in the equations related to non-perturbative renormalization and the structure of the massless unphysical states in the theory which is a priori unknown. The realization of the global gauge symmetries and the Kugo–Ojima confinement criterion crucially depend on this structure. For that reason functional equations have been supplemented by the appropriate boundary condition in the earlier literature on the scaling solution [12]. The restriction of the gauge field configuration space to the first Gribov region provides a simple example of boundary conditions which are not reflected in the form of the functional equations of the theory but need to be imposed in addition [11]. Another example is the Kugo–Ojima criterion which cannot be derived from the functional equations but needs to be added as a boundary condition. This then singles out the scaling solution with an infrared enhancement of the ghost propagator. Without this boundary condition, the functional equations admit both, the scaling solution and the decoupling solutions. Since these boundary conditions are imposed on unphysical degrees of freedom, they may be inconsequential for physical observables.

Indeed, the Gribov ambiguity and the associated freedom in globally completing the Landau gauge are well known to affect particularly the ghost propagator on the lattice [27–31, 35–37, 40–46]. For the volumes accessible in current simulations, it appears that this ambiguity is indeed closely related to the one-parameter freedom in the family of solutions to the functional equations: a direct correspondence between the Gribov ambiguity on the lattice and the one-parameter family of solutions to the functional equations of continuum quantum field theory is provided by the so-called Landau-B gauges [46]. These gauges correspond to different resolutions of the Gribov–Singer ambiguity. They are implemented by first selecting a target value, called the B parameter, for the ratio of ghost dressing functions evaluated at two widely separated momentum scales. An appropriate choice for the two momentum scales is the lowest accessible momentum on the lattice and some conveniently large momentum scale, such as the renormalization scale. This choice is made to resemble the non-perturbative freedom in choosing a boundary condition for the ghost propagator in the continuum studies. Then, on a configuration by configuration basis, many Gribov copies are generated to select the one where this ratio is closest to the target value B. The propagators, or other Green's functions, are calculated on these copies from the Monte-Carlo history of configurations.

Any finite number of Gribov copies leads to a finite set of proposed B values. In turn, for larger and larger lattices one can get close to any target value within a certain range depending on the lattice volume. We conclude that within this range the infrared value of the ghost dressing function can be chosen freely. An extreme case is the max-B gauge [46] in which the copy with the maximally enhanced ghost propagator is selected.

In general, it is of course practically impossible to find all Gribov copies for a given configuration. This limitation can cause some residual Gribov noise on top of the statistical fluctuations. In the case of the max-B gauge the result will be a lower bound for the maximally enhanced ghost propagator that is possible in any finite volume. In the present work, max-B gauge is implemented similarly to [46]. In order to reduce the effects of the lattice breaking of rotational invariance, the Euclidean $O(d)$ symmetry, the value of B for a given copy is determined by averaging over all representations for the lowest momentum, instead of using only one on-axis momentum as in [46]. Note also that the standard lattice implementation of the Landau gauge, the minimal Landau gauge, essentially gives the same results as choosing for B the expectation value of the ghost propagator ratio from all Gribov copies of all configurations [46].

4 Numerical results

The configurations have been obtained by generating randomly $\beta = 0$ configurations on symmetric lattices of size $L^d = (Na)^d$. Gauge fixing to the minimal Landau gauge in Sects. 4.1 and 4.2 has been performed using a stochastic overrelaxation method, see e.g. [72]. Fixing to the max-B gauge has been discussed in Sect. 3. Propagators are determined using a standard method, see, e.g., [73]. For the determination of the ghost propagator we also refer to Appendix A. A cylinder cut has been imposed to select momenta [74].

4.1 Two dimensions

The gluon propagator for various lattice sizes in $d = 2$ is shown in Fig. 1. Its value at vanishing momentum continues to decrease with the inverse lattice extension (Fig. 2), and therefore only a lower bound on a possible mass at zero momentum can be given. Power-law fits to the gluon propagator, according to (3a), yield a value of $\kappa_Z \approx 0.19$ at intermediate lattice momenta aq around 1, i.e. close to the scaling prediction of $\kappa_Z = 0.2$, with a tendency to decrease towards a value of 0.16 at large aq. At this point, this would all still be quite consistent with the scaling solution [11], which has also been concluded from previous lattice studies at finite coupling [65].

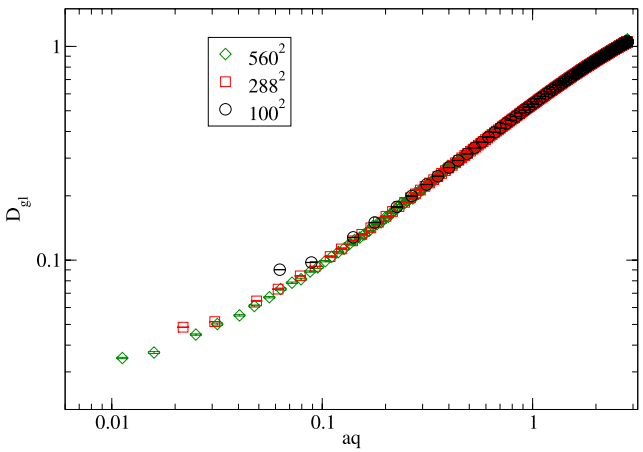

Fig. 1 Gluon propagator in $d = 2$ for different lattice sizes

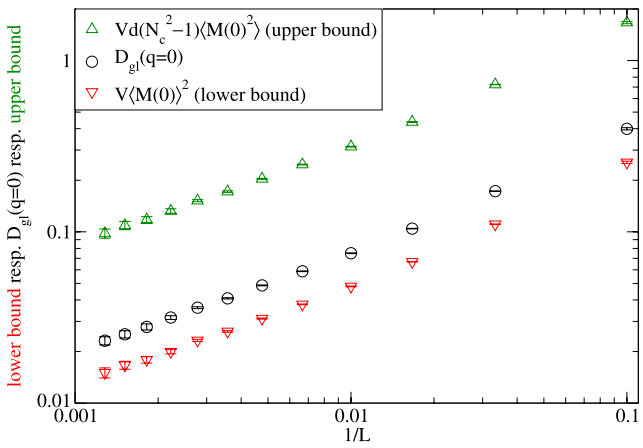

Fig. 2 Finite-volume behavior of the gluon propagator at zero momentum in $d = 2$. Also shown are the corresponding bounds from [32]

Our results for the ghost propagator, however, show much more significant deviations from this behavior. In particular, it appears that they cannot be reconciled with the infrared scaling hypothesis, as widely expected to hold at least for the two-dimensional theory [11, 12, 32, 34, 37, 64, 65]. In order to draw this conclusion, it is first of all crucial to have a sound statistical basis. In that respect it made a dramatic difference that we have employed a plane-wave method in obtaining the ghost propagator from the inversion of the Faddeev–Popov operator, instead of the point-source method used in [61]. The two methods are compared and discussed in more detail in Appendix A.

Fitting the ghost propagator, shown in Fig. 3, with a naive power-law ansatz at intermediate and large momenta, we extract a value of around $\kappa = 0.37$. This is significantly larger than the expected value of 0.2 [11, 65] and than the corresponding scaling exponent from the two-dimensional gluon propagator in this range. Moreover, the κ from the ghost propagator continues to increase as larger and larger lattice momenta are being used for the fit. A good way to illustrate this, and thus the absence of a stable scaling region for the ghost propagator in $d = 2$ dimensions, is to extract the value of κ locally, from just two momenta (i.e., momentum norms) via

$$(\kappa_Z)_{\text{local}} = \frac{1}{4}\left[\frac{\log D_{\text{gl}}(q_{i+\delta}) - \log D_{\text{gl}}(q_i)}{\log q_{i+\delta} - \log q_i} + (d-2)\right] \tag{12a}$$

$$(\kappa)_{\text{local}} = \frac{1}{2}\left[\frac{\log D_{\text{gh}}(q_i) - \log D_{\text{gh}}(q_{i+\delta})}{\log q_{i+\delta} - \log q_i} - 2\right]; \tag{12b}$$

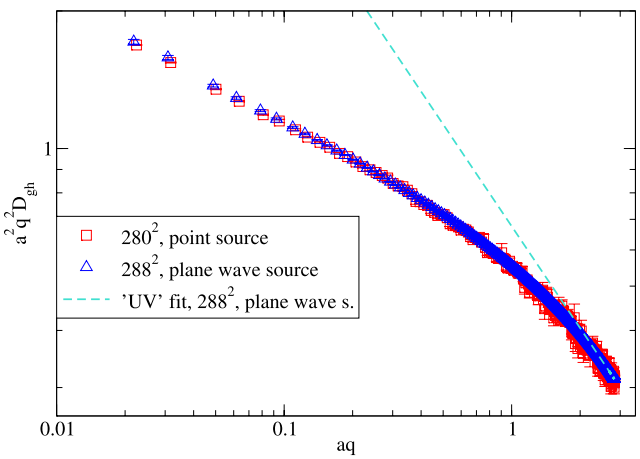

Fig. 3 Ghost dressing function in $d = 2$

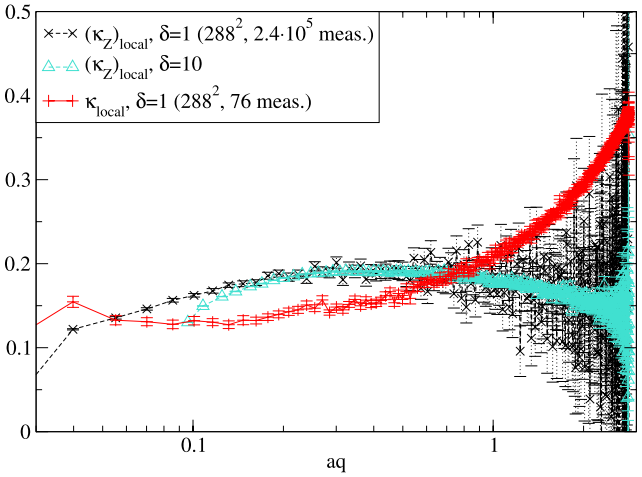

Fig. 4 'Local κ', i.e. extracted from q_i and $q_{i+\delta}$ from the 2D gluon (κ_Z) and ghost (κ) data, via (12a) and (12b)

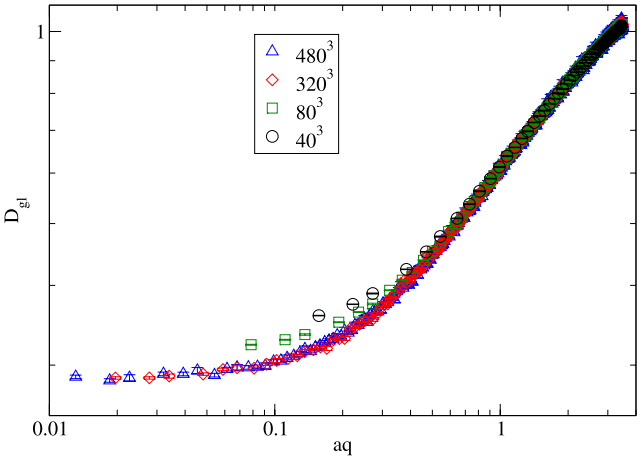

Fig. 5 Gluon propagator in $d = 3$ for various lattice sizes

see Fig. 4. The statistical errors have been estimated using a bootstrap analysis.[1] If anywhere, the locally defined exponent levels around relatively small lattice momenta of aq around 0.1 at a value which is several standard deviations below the gluon exponent there, and it continues to grow from there on towards larger momenta. Our results are clearly at odds with results at finite coupling on moderately sized lattices [65] supposedly showing a scaling behavior in agreement with predictions [11, 12].

4.2 Three dimensions

The gluon propagator in $d = 3$ is again relatively well-behaved. It shows a decoupling branch at small lattice momenta aq and a behavior resembling a scaling branch at large aq, see Fig. 5. While the decoupling branch still shows quite significant finite-volume effects, these are clearly not strong enough to permit a vanishing gluon propagator at zero momentum in the $L \to \infty$ limit, see Fig. 6.

As in two and four dimensions, the branch at large aq is consistent with a power law with an exponent κ_Z close to the value predicted by functional continuum methods, i.e., $\kappa_Z \approx 0.35$ versus the predicted 0.3976 [11], and in agreement with [61]. At large lattice momenta, the power-law exponent slightly decreases again, which is also evident from its local definition, see Fig. 7.

At the same time, Fig. 7 illustrates that things become murky again when analyzing the ghost propagator for potential power-law windows. Qualitatively, the situation is similar to that in $d = 2$ dimensions, the locally defined exponent continues to increase with increasing momenta and the ghost

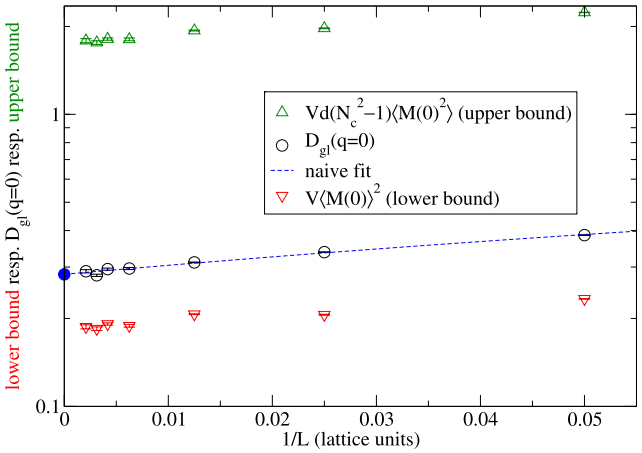

Fig. 6 Naive extrapolation of the gluon propagator in $d = 3$ at zero momentum to infinite lattice size. The decoupling branch persists in this limit. The bounds from [32] are also indicated

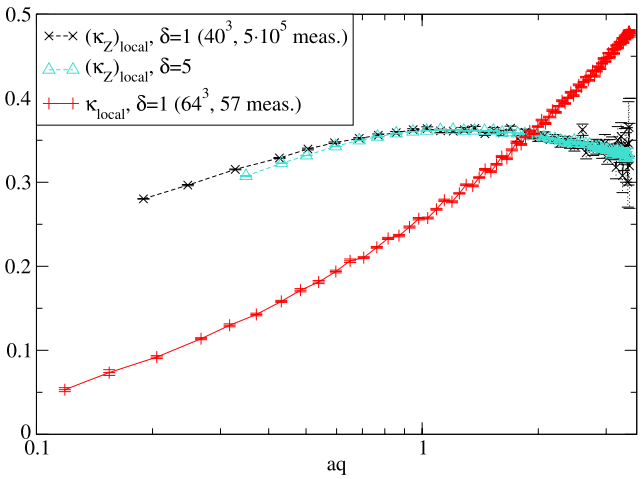

Fig. 7 'Local κ', as in Fig. 4 but for three dimensions

[1] A similar analysis was performed in three dimensions (see also our next subsection) already in [61] with the important difference, however, that the Faddeev–Popov operator was there inverted on a point source.

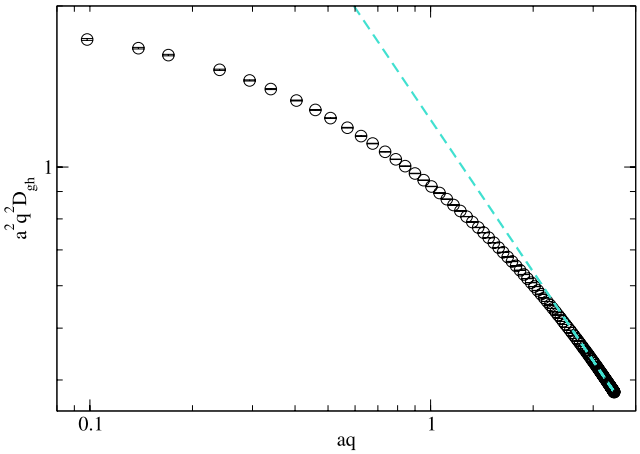

Fig. 8 Ghost dressing function for a 64^3 lattice. The dashed line is a power-law fit to large momenta

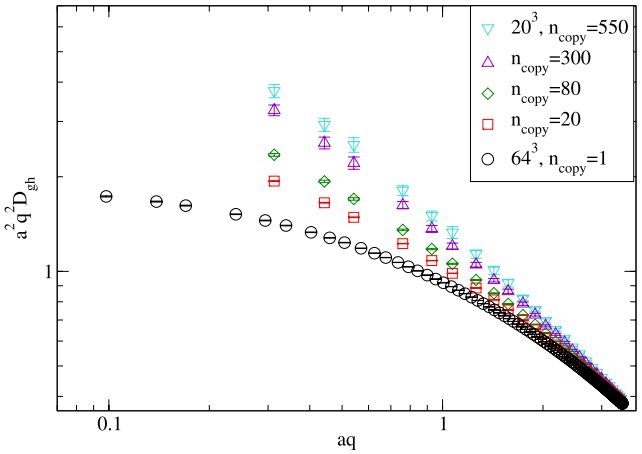

Fig. 9 Ghost dressing function in the max-B gauge for different numbers of Gribov copies taken into account

propagator cannot reasonably be interpreted as obeying a scaling behavior in any momentum range. The result for the ghost propagator itself is given in Fig. 8 which includes a fit over a maximal data set at large lattice momenta (extending up to the largest ones) such that $\chi^2/\mathsf{ndf} < 1$. The general conclusions are much the same as in the $d = 2$ case above.

4.3 The max-B gauge

The main aspect of the results that prevents a straightforward interpretation is the behavior of the ghost propagator which is most sensitive to the Gribov ambiguity. It therefore seems to be a natural question to ask what the influence is of this residual gauge freedom of the Landau gauge which can be used to change the ghost propagator as explained in Sect. 3. Here we deliberately choose the max-B Landau gauge of Sect. 3 in order to demonstrate the maximal effect. These are the first calculations at $\beta = 0$ in this gauge. In the strong-coupling limit one generates random gauge orbits for which the typical number of Gribov copies is extremely large. Moreover, this number is expected to grow exponentially with the number of lattice sites N^d. It will therefore be practically impossible to find even a significant fraction of all copies on large lattices. We therefore restrict the analysis to relatively modest lattice sizes such as 48^2 and 20^3. It would have been possible of course that the results saturated rather quickly with the number of Gribov copies taken into account, as it appeared to be the case in calculations at $\beta > 0$ [28, 30]. This does not happen here, however, at least not for the up to 600 copies per orbit analyzed on these lattices. As one can see below in Fig. 12, in particular the low-momentum values of the ghost propagator continue to grow as more and more Gribov copies are included in the max-B gauge.

Our results for the ghost propagator in $d = 3$ dimensions are shown in Fig. 9. We observe a strong increase in the

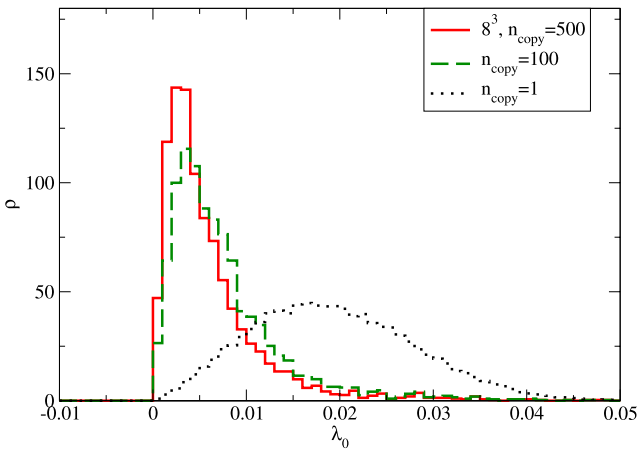

Fig. 10 Effect of the max-B-gauge on the lowest nontrivial (i.e., non-vanishing) FPO eigenvalue as a function of included Gribov copies. Entries in the histogram correspond to the lowest eigenvalue on different configurations for the Gribov copy with the most divergent ghost propagator

ghost dressing function with the number of Gribov copies n_{copy} included per orbit in the search for the max-B gauge. The observed enhancement in the ghost dressing function at low momenta comes along with a significant shift in the spectrum of the lattice Faddeev–Popov operator (FPO), as one would expect. This is illustrated on an even smaller lattice in Fig. 10. The strong correlation between the lowest Faddeev–Popov eigenvalue λ_0, omitting the three trivial zero eigenmodes, and the ghost propagator at lowest non-vanishing momentum is seen in Fig. 11 (see also [75]).

It seems surprising that the ghost propagator in the max-B gauge appears to show no sign of saturation with the number of Gribov copies taken into account, even on these small lattices and in both, two and three dimensions, as illustrated in Fig. 12. It appears not likely that the ghost propagator should increase without bound as the number of

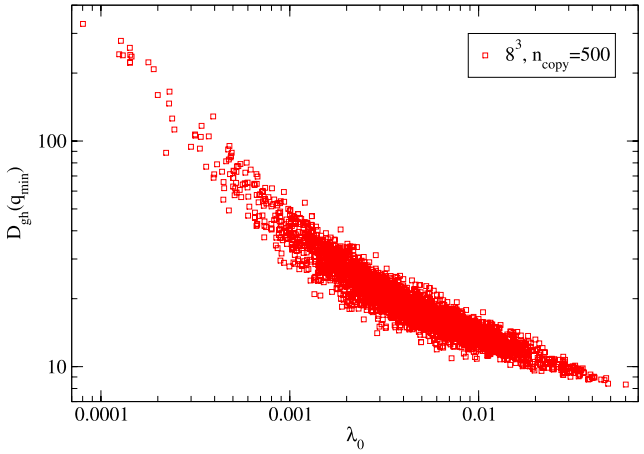

Fig. 11 Strong correlation between lowest FPO eigenvalue and ghost propagator at lowest non-vanishing momentum (in the max-B gauge)

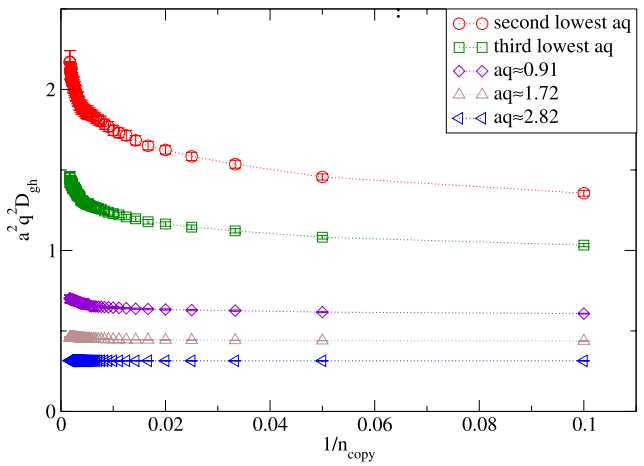

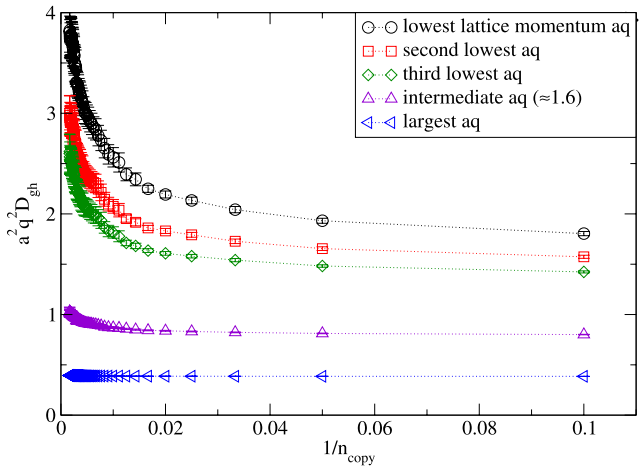

Fig. 12 Ghost dressing function vs. inverse number of Gribov copies for the max-B gauge. *Top*: for $d = 2$ dimensions and a 48^2 lattice. *Bottom*: for $d = 3$ dimensions and a 20^3 lattice. Lines are drawn to guide the eye

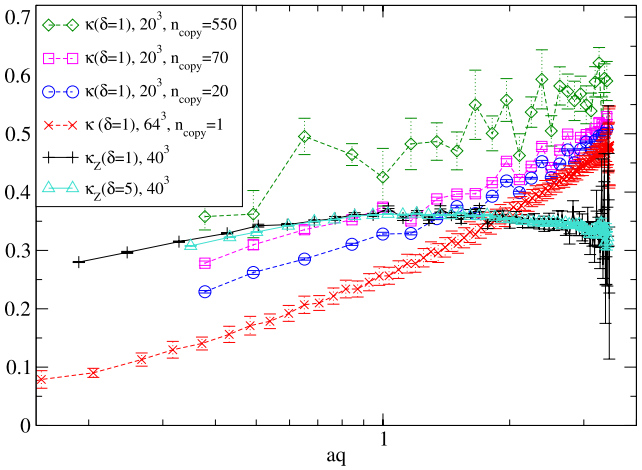

Fig. 13 Local κ_Z resp. κ from the max-B gauge

copies is further increased in a finite volume, but we are obviously still far from having sampled sufficiently many to conclude that we could reach a stable limit. We conclude that Gribov copies do have an enormous effect on the low-momentum behavior of the ghost propagator. This is also reflected in the corresponding κ's as shown in Fig. 13.

It should be noted that by choosing instead of the maximum value of the ghost propagator a finite value for B, it is possible to generate any ghost propagator in between the one of minimal Landau gauge and the one in the max-B gauge. In fact, it is also possible to select a ghost propagator which is smaller than the one in minimal Landau gauge [46].

However, our primary interest in employing the max-B gauge is to investigate a potential fixed-point behavior in the running coupling, an issue to which we now turn.

4.4 Running coupling

Let us emphasize that an increase of κ from the ghost propagator towards large lattice momenta is actually also apparent from the $d = 4$ data presented already in [42–44], as shown explicitly in Fig. 14. But it is important to notice that in this case, unlike in $d = 2$ and $d = 3$, Fig. 12, κ from the ghost data does not rise above κ_Z, i.e., the ghost exponent extracted from the gluon data. This manifests itself in a different behavior of the effective running coupling (9). As reported in [42, 43], in $d = 4$, α_s grows monotonically as a function of aq and approaches a value $\alpha_c \approx 4$ from below, which is close to the value $\alpha_c \approx 4.46$ predicted in [12].

The behavior we observe here in minimal Landau gauge in $d = 2$ and $d = 3$ differs surprisingly: The behavior at large lattice momenta is notably different from the four-dimensional case, see Fig. 15. This is obviously a joint consequence of the behavior of κ and κ_Z (Figs. 4 respectively 7) and the fact that from (9)

$$\alpha_e \propto \left(q^2\right)^{2(\kappa_Z - \kappa)}. \tag{13}$$

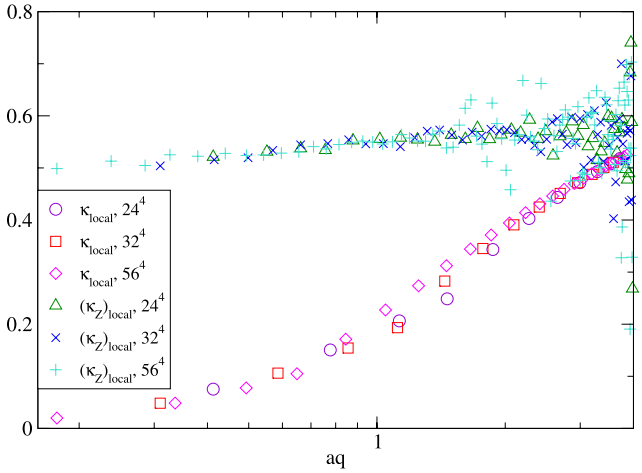

Fig. 14 'Local κ', as in Fig. 4 but for $d = 4$ dimensions; see [43] for the corresponding propagator results. For the ghost propagator, not all momenta eligible under the cylinder cut have been used here. The exponent κ_Z from the gluon data is virtually constant except for the smallest lattice momenta. Error bars are relatively small and not shown

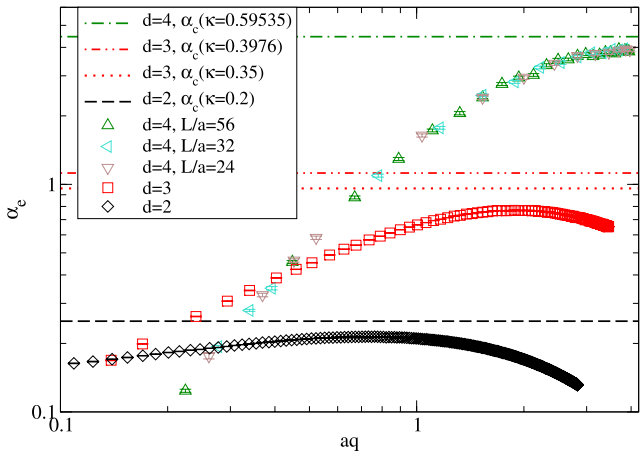

Fig. 15 α_e in $d = 2$, $L = 288$, and $d = 3$, $L = 64$, as well as from various lattice sizes in $d = 4$

In $d = 2$ and 3, where the local κ grows monotonically and intersects κ_Z at some aq, see Figs. 4 and 7, α_e reaches a maximum near the respective lattice momentum, as implied by (13). Comparing the results to the predictions from [12], we find the maximum of α_e is approx. 85% of the predicted (constant) value of α_c in $d = 2$ and $\approx 70\%$ in $d = 3$, instead of $\approx 90\%$ in $d = 4$. This refers to the prediction for α_c given the standard values of κ, i.e. 0.3976... in $d = 3$ and 0.2 in $d = 2$. The situation slightly improves if the value of the predicted α_c is calculated instead with the κ values actually observed on the lattice. In $d = 3$, this amounts to choosing $\kappa = 0.35$, see Fig. 15.

While the behavior of α_e in $d = 2$ and 3 is surprising and not amenable to an immediate explanation, it is interesting to note that the maximum of $\alpha_s(aq)$ shows a monotonic behavior from $d = 2$ to $d = 4$, i.e., it is shifted to larger aq. This follows the general pattern observed also at finite β: the window in which a scaling-like behavior is observed extends to much smaller momenta in two dimensions than in three dimensions, before the effective masses begin to dominate. In four dimensions, finally, the window becomes so small that almost no scaling-like behavior can yet be observed. The same mechanism seems here to shift the observed maximum to ever smaller values of aq.

A possible explanation for these results would be that at large aq discretization effects are visible while at small aq a Gribov copy effect causes the deviation of α_e from the continuum solution ($\alpha_e = \alpha_c = \text{const}$).

The second possibility motivates us to investigate the effect of the max-B gauge with a growing number of copies on α_e. We have used up to 600 Gribov copies per configuration on a 20^3 lattice. The effect on the ghost propagator is strong, as is apparent from Fig. 12 (bottom) in the previous subsection. We observe no 'saturation'.

By virtue of (9), this effect induces an even stronger change in the running coupling (see Fig. 16), which is far from being balanced by a similarly strong change in the gluon propagator. In fact, it was already stated in [46] that the effect of choosing the max-B gauge on the gluon propagator is relatively small for the employed lattice sizes.

Since the result overshoots the prediction this implies that it is possible to select a value of B such that actually an infrared finite coupling could be generated. Such a choice leads to essentially the same behavior, as is seen when artificially the number of copies is restricted to ≈ 70 in $d = 3$. This is equivalent to the statement that the locally extracted values of κ and κ_Z are consistent within errors in this region, see Fig. 13.

There is currently no fully satisfactory explanation for the behavior of the running coupling and the observed overscaling. Even though a $n_{\text{copy}} \to \infty$ extrapolation is not at all feasible from the current data, the result in this limit on a 20^3 lattice will be at odds with the continuum prediction for α_c. One possible solution might be to consider larger lattices.

We have done similar simulations for the two-dimensional case, again initially on a small lattice (48^2). The qualitative picture is similar to the three-dimensional case, see Fig. 16, as a scaling region is also absent. As noted above, this is surprising. In particular, when considering the scaling behavior observed in two dimensions [32, 34, 37, 65] at volumes where only very few Gribov copies are present [45, 46].

Regarding the presence of possible discretization artifacts at large momenta, one possible concern in this context is the lattice breaking of rotational invariance at $\beta = 0$. The fact that the dressing functions on the lattice are invariant under the lattice isometries does not imply that they are also invariant under the Euclidean $O(d)$ symmetry in d dimensions. This implies that the dressing functions depend on the

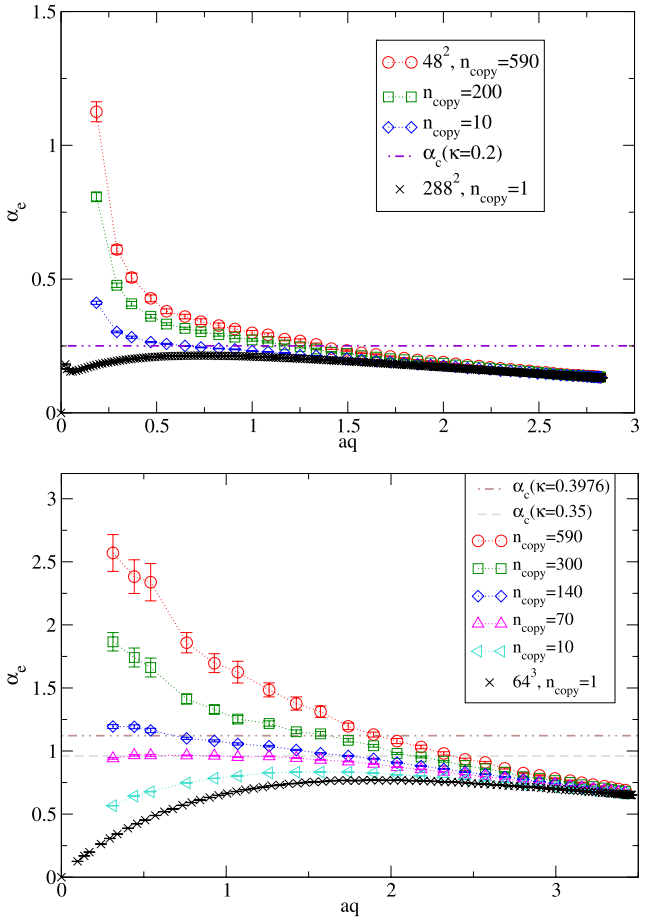

Fig. 16 max-B gauge: Very strong change in the running coupling, especially at small lattice momenta, as the number of Gribov copies increases. *Top*: for $d = 2$ dimensions and a 48^2 lattice. *Bottom*: for $d = 3$ dimensions and a 20^3 lattice

orbits generated by the lattice isometries, but there are different such orbits that correspond to the same $O(d)$ orbit classified by the magnitude of momentum q^2 (see, e.g., [76]). These differences are of higher order in the lattice spacing and would vanish in the continuum limit. There is no suppression of these differences in the strong-coupling limit, however, and they will therefore show up in differences of dressing functions evaluated along different momentum directions. We assess these effects of the lattice breaking of rotational invariance in Appendix B. They are not as dramatic as the Gribov effects, but the tendency of the fixed-point couplings to decrease at large lattice momenta is within the systematic uncertainty due to these effects.

5 Conclusions

We close with a summary of our main results and a discussion of the consequences. In the present work we have qualitatively extended previous studies on the strong-coupling limit $\beta = 0$ of Landau gauge SU(2) Yang–Mills theory on the lattice. In two and three dimensions we have shown that the Gribov ambiguity is rather strong. It especially affects the ghost propagator which neither uniquely shows a scaling nor a decoupling behavior for small lattice momenta. Indeed, subject to the number of gauge copies used, it even shows over-scaling for small and intermediate momenta. Our $\beta = 0$ results also indicate that over-scaling can be achieved for any finite lattice if enough gauge copies are taken into account. However, in the continuum over-scaling is prohibited by the uniqueness proof put forward in [15, 16, 70]. It is not part of the one-parameter family of solutions [7, 57] and might hint at the scaling solution as the limit of the over-scaling lattice Landau gauge fixing.

In any case, the above results are in marked contrast to the results in previous works where only a decoupling-type solution was obtained at low momenta, see [42–44, 61]. Evidently the interpretation of the $\beta = 0$ results needs to be seriously reconsidered.

At large lattice momenta, the ghost propagator does not naively exhibit scaling, as its local scaling coefficient, κ, rises monotonically. This is neither a scaling behavior, nor is it a decoupling-type behavior. Indeed, a logarithmic fit appears to be possible, and has been related to similar fits for the decoupling solution in the continuum [61]. Note, however, that this similarity is superficial because the prefactor of the logarithmic term has the wrong sign. A naive extrapolation to finite β and the infinite-volume limit would lead to a pole at some finite momentum. On the other hand, the gluon propagator shows approximate scaling and hence a qualitatively different behavior from the ghost. Such a different behavior would not be expected for a decoupling-type solution. A possible explanation for these surprising results are strong but not unexpected discretization effects associated with the unphysical $\beta \to 0$ limit at large aq, see Appendix B.

Our results are best summarized in Fig. 16 for the running coupling. It is the only RG-invariant product of the two dressing functions and is rather sensitive to the global aspects of the gauge fixing. Its behavior at small lattice momenta confirms that the Gribov ambiguity is much stronger than expected on the basis of previous results. Extrapolating to finite β in four dimensions, we conclude that a resolution of the Gribov ambiguity requires far more computational power than presently employed [32–34, 36, 37, 77]. In particular this implies that the present data cannot be used to exclude any subset of infrared solutions. It is all within the uncertainties due to the Gribov ambiguity. Indeed, we are confident that our data together with other lattice and continuum results [7, 17, 22, 25, 45, 47, 50–59, 71, 78] can be unified in an overall picture of Landau gauge Yang–Mills theory as put forward in [7, 46, 47, 57]. Its further understanding would certainly provide more insight into the confining physics.

Acknowledgements We thank A. Cucchieri, C.S. Fischer, T. Mendes, M. Müller-Preussker and I. Stamatescu for discussions and comments on the manuscript. This work is supported by the Helmholtz Alliance HA216/EMMI and the Helmholtz International Center for FAIR within the LOEWE program of the State of Hessen. A.M. was supported by the FWF under grant number M1099-N16, and A.S. by the Australian Research Council and the SFB/TR 55. D.S. acknowledges support by the Landesgraduiertenförderung Baden-Württemberg via the Research Training Group "Simulational Methods in Physics". The numerical simulations were carried out on bwGRiD (http://www.bw-grid.de), member of the German D-Grid initiative, on the compute cluster of the ITP, University of Heidelberg, and partly at the HPC cluster of the University of Graz.

Appendix A: Plane-wave vs. point source

We expand here the study of [73], which showed that the method to obtain the inverse of the Faddeev–Popov operator to calculate the ghost propagator has quite an impact on the statistical accuracy of the calculation. Especially, for extracting information about the local behavior it is advantageous to employ a plane-wave source [40] instead of a point source [79] for the conjugate gradient method used to invert the operator. This means that the Faddeev–Popov operator is inverted on a vector of plane waves, $s_b^{a,x}(k) = \delta^{ab} e^{ik\cdot x}$, instead of a point source, $s_b^{a,x} = \delta^{ab}(\delta_{x,0} - 1/V)$, with $k \cdot x = 2\pi \sum_\mu k_\mu x_\mu / L_\mu$.

The contrast is illustrated in Fig. 17, which already suggests that the point source makes a power-law fit at large lattice momenta, and thereby the identification of a scaling region with an unique exponent κ, considerably more difficult. This statement can be made more precise, e.g., by performing power-law fits at large lattice momenta and comparing the respective values of χ^2/ndf. The reason is that a plane-wave source averages over all possible inversion points, and therefore provides a volume-factor less noise than a point source. The drawback of a plane-wave source is that an inversion is required for every momentum value.

This problem is further illustrated in Fig. 18 for a locally defined κ, in contrast to Fig. 4 (plane-wave source). Of course, in the limit of infinite statistics, both methods will yield the same result. Using a point source to determine the value of κ at large momenta, a value of 0.31 would be obtained.

Similar considerations apply in all dimensions. The result for the point-source method in three dimensions is shown in Fig. 19. The fluctuations are greatly enhanced compared to the plane-wave result shown in Fig. 8. Even with $N \in \mathcal{O}(10^5)$ configurations, they are still larger than in the latter

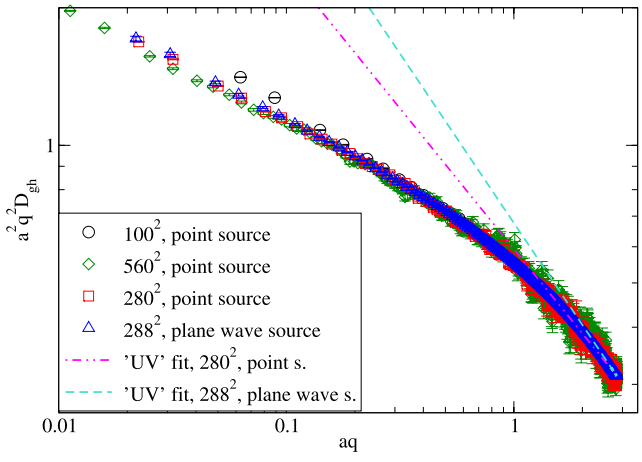

Fig. 17 Ghost dressing function in $d = 2$. In order to draw conclusions about the behavior at large lattice momenta, the plane-wave source method is clearly preferable to the point-source method: only 76 meas. on 288^2 (plane-wave source) vs. ≈ 37000 on 280^2 (point source) yield much less fluctuations

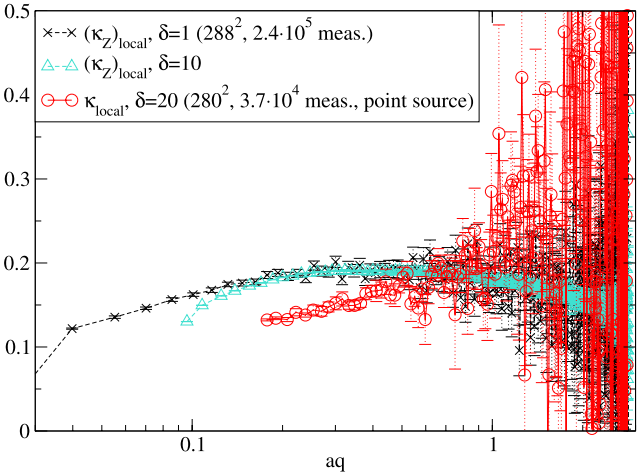

Fig. 18 'Local κ' for a point source from 37000 measurements and calculated from (cylinder cut) momentum norms that are $\delta = 20$ indices apart. Compare to the result from a plane-wave source with 76 meas. at $V = 288^2$ in Fig. 4

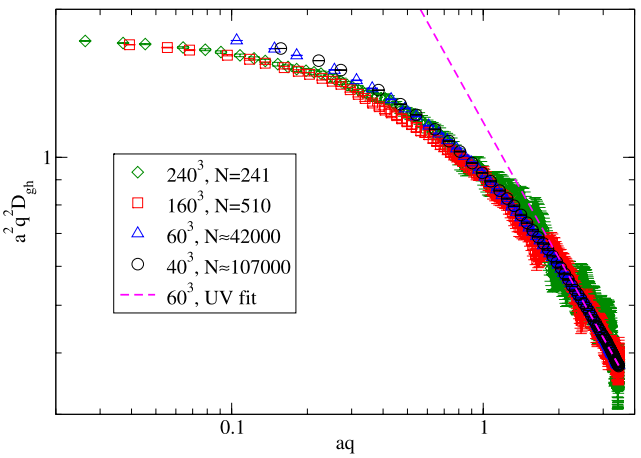

Fig. 19 The ghost dressing function in three dimensions using the point-source method. The numbers N of independent configurations are given in the legend. For an explanation of the wiggles at large momenta see [73]

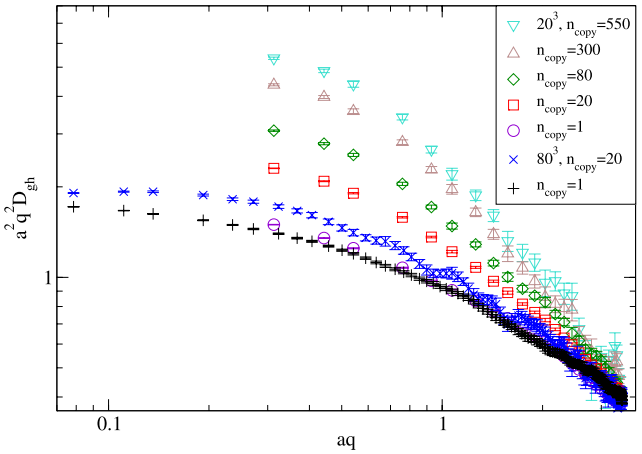

Fig. 20 Finite-volume effect for minimal Landau gauge and for max-B gauge with various numbers of copies. Point-source method

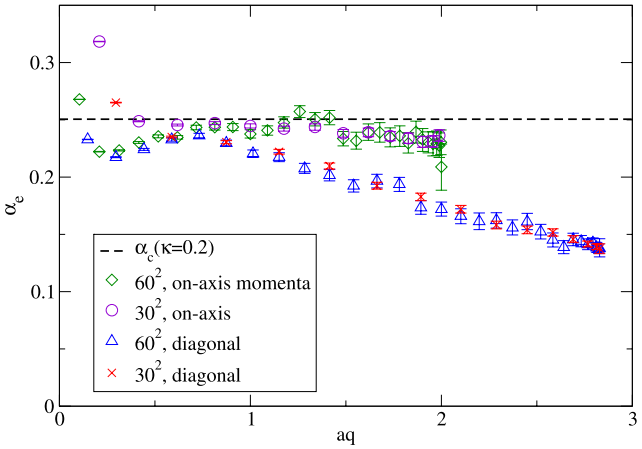

Fig. 21 Effective running coupling in $d = 2$ for two different choices of lattice momenta

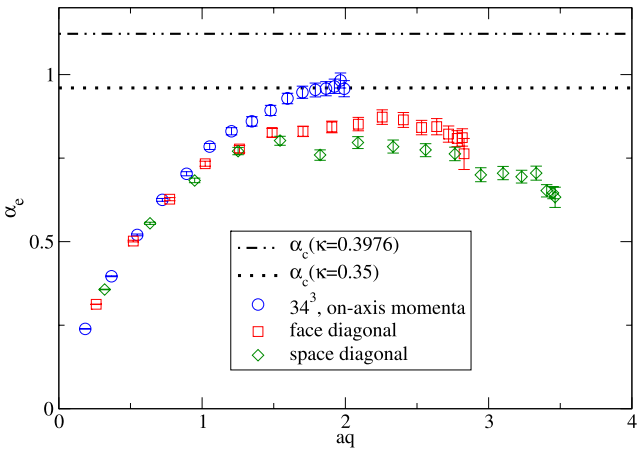

Fig. 22 Effective running coupling in $d = 3$ for three different choices of lattice momenta

case. Correspondingly, the region where a power-law fit at large aq with $\chi^2/\mathrm{ndf} < 1$ is possible, is much smaller.

There is also a note in conjunction with the max-B gauge employed. The ghost propagator using the point source exhibits much larger statistical fluctuations. Consequently, when triggering on large fluctuations, as when implementing the max-B gauge, it is likely that in a sample of finite statistics the ghost propagator will be larger in the max-B gauge than when using a plane-wave source. Due to its inherent averaging over the lattice the plane-wave source method smooths these exceptional fluctuations in many more cases. Only when volume-times more statistics have been used for the point-source method than for the plane-wave source method, a similar smoothing effect can be expected to take place. Again, in the limit of infinite statistics both methods will then yield the same result. A measure of this, aside from the ghost propagator directly, is the comparison of average vs. median. At the present statistics, in both cases both measures significantly deviate but the difference is much larger for the point-source method than for the plane-wave source method. Also, when using the median instead of the average the results for both methods are more similar.

As an example, the results at finite statistics for the point-source method are shown in Fig. 20. Comparing to Fig. 9 from the main text displays exactly this point.

Appendix B: Discretization effects

As noted above, we have usually applied a cylinder cut to the momenta. In order to obtain a rough estimate of possible discretization artifacts, we have also calculated the running coupling for the opposite case of on-axis momenta, $k_i = k\delta_{ij}$ for all fixed j. Interestingly, the effective running coupling thus obtained is compatible with a constant value at large lattice momenta close to the continuum prediction [12], see Fig. 21. These data have been produced with the point-source method, which suffices to clearly observe the qualitative effect. Data at diagonal momenta, which form a subset of the momenta surviving the cylinder cut, are shown for comparison. In $d = 3$, the difference between the choices of momenta is again clearly visible, see Fig. 22, though less pronounced than in the lower-dimensional case. This suggests an even weaker effect for $d = 4$, where indeed the running coupling has been found to tend towards a constant value at large aq [42, 43]. These early results underline the serious discretization problem faced at large aq at $\beta = 0$ and call for further investigations along these lines, e.g. in max-B gauge.

References

1. R. Alkofer, L. von Smekal, Phys. Rep. **353**, 281 (2001). hep-ph/0007355

2. R. Alkofer, J. Greensite, J. Phys. G **34**, S3 (2007). hep-ph/0610365
3. R. Alkofer, W. Detmold, C.S. Fischer, P. Maris, Phys. Rev. D **70**, 014014 (2004). hep-ph/0309077
4. J. Braun, H. Gies, J.M. Pawlowski, PoS **CONFINEMENT8**, 044 (2008). 0708.2413
5. V.N. Gribov, Nucl. Phys. B **139**, 1 (1978)
6. I.M. Singer, Commun. Math. Phys. **60**, 7 (1978)
7. C.S. Fischer, A. Maas, J.M. Pawlowski, Ann. Phys. **324**, 2408 (2009). 0810.1987
8. P. Boucaud et al., J. High Energy Phys. **06**, 099 (2008). 0803.2161
9. L. von Smekal, R. Alkofer, A. Hauck, Phys. Rev. Lett. **79**, 3591 (1997). hep-ph/9705242
10. L. von Smekal, A. Hauck, R. Alkofer, Ann. Phys. **267**, 1 (1998). hep-ph/9707327
11. D. Zwanziger, Phys. Rev. D **65**, 094039 (2002). hep-th/0109224
12. C. Lerche, L. von Smekal, Phys. Rev. D **65**, 125006 (2002). hep-ph/0202194
13. J.M. Pawlowski, D.F. Litim, S. Nedelko, L. von Smekal, Phys. Rev. Lett. **93**, 152002 (2004). hep-th/0312324
14. R. Alkofer, C.S. Fischer, F.J. Llanes-Estrada, Phys. Lett. B **611**, 279 (2005). hep-th/0412330
15. C.S. Fischer, J.M. Pawlowski, Phys. Rev. D **75**, 025012 (2007). hep-th/0609009
16. M.Q. Huber, R. Alkofer, C.S. Fischer, K. Schwenzer, Phys. Lett. B **659**, 434 (2008). 0705.3809
17. D. Zwanziger, 0904.2380 (2009)
18. A.C. Aguilar, A.A. Natale, J. High Energy Phys. **08**, 057 (2004). hep-ph/0408254
19. A.C. Aguilar, D. Binosi, J. Papavassiliou, PoS **LC2008**, 050 (2008). 0810.2333
20. A.C. Aguilar, D. Binosi, J. Papavassiliou, Phys. Rev. D **78**, 025010 (2008). 0802.1870
21. P. Boucaud et al., J. High Energy Phys. **06**, 001 (2006). hep-ph/0604056
22. P. Boucaud et al., J. High Energy Phys. **06**, 012 (2008). 0801.2721
23. D. Dudal, S.P. Sorella, N. Vandersickel, H. Verschelde, Phys. Rev. D **77**, 071501 (2008). 0711.4496
24. D. Dudal, J.A. Gracey, S.P. Sorella, N. Vandersickel, H. Verschelde, Phys. Rev. D **78**, 065047 (2008). 0806.4348
25. D. Binosi, J. Papavassiliou, Phys. Rep. **479**, 1 (2009). 0909.2536
26. A.C. Aguilar, D. Binosi, J. Papavassiliou, J. Rodriguez-Quintero, Phys. Rev. D **80**, 085018 (2009). 0906.2633
27. T.D. Bakeev, E.-M. Ilgenfritz, V.K. Mitrjushkin, M. Müller-Preussker, Phys. Rev. D **69**, 074507 (2004). hep-lat/0311041
28. P.J. Silva, O. Oliveira, Nucl. Phys. B **690**, 177 (2004). hep-lat/0403026
29. I.L. Bogolubsky, G. Burgio, M. Muller-Preussker, V.K. Mitrjushkin, Phys. Rev. D **74**, 034503 (2006). hep-lat/0511056
30. A. Sternbeck, E.-M. Ilgenfritz, M. Müller-Preussker, A. Schiller, Phys. Rev. D **72**, 014507 (2005). hep-lat/0506007
31. I.L. Bogolubsky et al., Phys. Rev. D **77**, 014504 (2008). 0707.3611
32. A. Cucchieri, T. Mendes, Phys. Rev. Lett. **100**, 241601 (2008). 0712.3517
33. A. Sternbeck, L. von Smekal, D.B. Leinweber, A.G. Williams, PoS **LAT2007**, 340 (2007). 0710.1982
34. A. Cucchieri, T. Mendes, Phys. Rev. D **78**, 094503 (2008). 0804.2371
35. V.G. Bornyakov, V.K. Mitrjushkin, M. Muller-Preussker, Phys. Rev. D **79**, 074504 (2009). 0812.2761
36. I.L. Bogolubsky, E.-M. Ilgenfritz, M. Müller-Preussker, A. Sternbeck, Phys. Lett. B **676**, 69 (2009). 0901.0736
37. J.M. Pawlowski, D. Spielmann, I.-O. Stamatescu, Nucl. Phys. B **830**, 291 (2010). 0911.4921
38. O. Oliveira, P.J. Silva, 0910.2897 (2009)
39. O. Oliveira, P.J. Silva, 0911.1643 (2009)
40. A. Cucchieri, Nucl. Phys. B **508**, 353 (1997). hep-lat/9705005
41. A. Cucchieri, Nucl. Phys. B **521**, 365 (1998). hep-lat/9711024
42. A. Sternbeck, L. von Smekal, PoS **LATTICE2008**, 267 (2008). 0810.3765
43. A. Sternbeck, L. von Smekal, 0811.4300 (2008)
44. A. Sternbeck, L. von Smekal, PoS **CONFINEMENT8**, 049 (2008). 0812.3268
45. A. Maas, Phys. Rev. D **79**, 014505 (2009). 0808.3047
46. A. Maas, 0907.5185 (2009)
47. J.M. Pawlowski, L. von Smekal, in preparation (2010)
48. M. Tissier, N. Wschebor, Phys. Rev. D **79**, 065008 (2009). 0809.1880
49. M. Tissier, N. Wschebor, 0901.3679 (2009)
50. A.J. Gomez, M.S. Guimaraes, R.F. Sobreiro, S.P. Sorella, Phys. Lett. B **683**, 217 (2010). 0910.3596
51. S.P. Sorella, Phys. Rev. D **80**, 025013 (2009). 0905.1010
52. K.-I. Kondo, 0909.4866 (2009)
53. K.-I. Kondo, 0907.3249 (2009)
54. K.-I. Kondo, 0905.1899 (2009)
55. K.-I. Kondo, Phys. Lett. B **678**, 322 (2009). 0904.4897
56. H. Neuberger, Phys. Lett. B **183**, 337 (1987)
57. L. von Smekal, 0812.0654 (2008)
58. L. von Smekal, A. Jorkowski, D. Mehta, A. Sternbeck, PoS **CONFINEMENT8**, 048 (2008). 0812.2992
59. L. von Smekal, D. Mehta, A. Sternbeck, A.G. Williams, PoS **LAT2007**, 382 (2007). arXiv:0710.2410 [hep-lat]
60. D. Mehta, A. Sternbeck, L. von Smekal, A.G. Williams, PoS **QCD-TNT09**, 025 (2009). 0912.0450
61. A. Cucchieri, T. Mendes, Phys. Rev. D **81**, 016005 (2010). 0904.4033
62. A. Cucchieri, Phys. Lett. B **422**, 233 (1998). hep-lat/9709015
63. P. de Forcrand, M. Fromm, 0907.1915 (2009)
64. D. Dudal, S.P. Sorella, N. Vandersickel, H. Verschelde, Phys. Lett. B **680**, 377 (2009). 0808.3379
65. A. Maas, Phys. Rev. D **75**, 116004 (2007). 0704.0722
66. C.S. Fischer, B. Grüter, R. Alkofer, Ann. Phys. **321**, 1918 (2006). hep-ph/0506053
67. A. Maas, in preparation (2010)
68. R. Alkofer, L. von Smekal, Nucl. Phys. A **680**, 133 (2000). hep-ph/0004141
69. J.C. Taylor, Nucl. Phys. B **33**, 436 (1971)
70. C.S. Fischer, J.M. Pawlowski, Phys. Rev. D **80**, 025023 (2009). 0903.2193
71. M.Q. Huber, R. Alkofer, S.P. Sorella, Phys. Rev. D **81**, 065003 (2010). 0910.5604
72. A. Cucchieri, T. Mendes, Nucl. Phys. B **471**, 263 (1996). hep-lat/9511020
73. A. Cucchieri, A. Maas, T. Mendes, Phys. Rev. D **74**, 014503 (2006). hep-lat/0605011
74. D.B. Leinweber, J.I. Skullerud, A.G. Williams, C. Parrinello (UKQCD), Phys. Rev. D **60**, 094507 (1999). hep-lat/9811027
75. A. Sternbeck, E.M. Ilgenfritz, M. Muller-Preussker, Phys. Rev. D **73**, 014502 (2006). hep-lat/0510109
76. F. de Soto, C. Roiesnel, J. High Energy Phys. **09**, 007 (2007). 0705.3523
77. C.S. Fischer, A. Maas, J.M. Pawlowski, L. von Smekal, Ann. Phys. **322**, 2916 (2007). hep-ph/0701050
78. L. von Smekal, M. Ghiotti, A.G. Williams, Phys. Rev. D **78**, 085016 (2008). 0807.0480
79. P. Boucaud et al., Phys. Rev. D **72**, 114503 (2005). hep-lat/0506031